Environmental Engineering and Management Journal

December 2021, Vol. 20, No. 12, 2049-2060
http://www.eemj.icpm.tuiasi.ro/; http://www.eemj.eu

"Gheorghe Asachi" Technical University of Iasi, Romania

COMPARATIVE STUDY ON ADSORPTION OF BASIC BLUE 41 (BB41) DYE FROM AQUEOUS SOLUTION ONTO TWO SGOs

Aysan Hassanzadeh Bavojdan[1], Mohammad Reza Alavi Moghaddam[1*], Elaheh Kowsari[2]

[1]*Civil and Environmental Engineering Department, Amirkabir University of Technology (Tehran Polytechnic), Hafez Ave., Tehran, 15875-4413, Iran*
[2]*Department of Chemistry, Amirkabir University of Technology (Tehran Polytechnic), Hafez Ave., Tehran, 15875-4413, Iran*

Abstract

The main purpose of the present research was a comparative study of two functionalized sulfonated graphene oxide (SGO) for removal of selected pollutant (Azo-Cationic Basic Blue 41 dye) in aqueous solution. The two nano-adsorbents (GO/1,4-butane sultone (SGO_1) and GO/1,3-propane sultone (SGO_2)) were synthesized, and characterized by Scanning Electron Microscope (SEM), Brunauer-Emmett-Teller (BET), X-ray Crystallography (XRD), Raman spectroscopic, and Fourier-Transform Infrared Spectroscopy (FTIR) analysis. The adsorption process of BB41 dye onto two nano-adsorbents was investigated. Selected parameters including initial solution pH, initial BB41 concentration, adsorbent dose, and contact time were evaluated. pH= 8, initial BB41 dye concentration= 50 and 100 mg/L, adsorbent dose= 0.2 and 0.15 g/L and contact time= 60 and 30 minute at room temperature, were the optimum values of the parameters for SGO_1 and SGO_2, respectively. The maximum adsorption capacity with SGO_1 and SGO_2 (assuming minimum removal of 80%) were found to be 274 and 434 mg/g. The study of isotherm and kinetics showed that both nano-adsorbents followed the Langmuir equilibrium model and were best fitted to the pseudo-second-order model. Moreover, according to the thermodynamic analysis the adsorption process, at all analyzed temperatures, was endothermic. The SGO_2 nano-adsorbent had shown higher efficiency than the SGO_1 nano-adsorbent during four cycles of the regeneration/ recovery investigation.

Key words: dye adsorption, isotherm, process kinetic, sulfonated graphene oxide, thermodynamics

Received: October, 2020; Revised final: April, 2021; Accepted: October, 2021; Published in final edited form: December, 2021

1. Introduction

Apart from having a destructive effect on the environment, synthetic dyes, which are used in different industries, have also been identified as carcinogenic and mutagenic materials (Zarezadeh-Mehrizi and Badiei, 2014). Synthetic dyes are a major pollutant of water, an essential component of life and the Earth's ecosystem. It is, therefore, crucial to remove dyes from wastewater efficiently in order to protect human health as well as the quality of the environment (Basheer, 2018a, 2018b; Mubarak et al., 2021; Shoushtarian et al., 2020). The Basic Blue 41 (BB41) azo-cationic dye is particularly suitable for acrylic substrates dyeing due to its low-cost and persistence; also, it can be applied to some polyester and polyamide types, cotton, viscose, and wool (Roulia and Vassiliadis, 2005). BB41 is a non-biodegradable dye due to its aromatic structure. Therefore, it remains in the environment for a long time (Zarezadeh-Mehrizi and Badiei, 2014).

There are various methods to remove BB41 from aqueous solutions, such as adsorption (Boudechiche et al., 2019; Jiang et al., 2013; Kooli et al., 2015; Mahmoodi et al., 2012; Regti et al., 2017), photocatalytic degradation (Mahmoodi and Abdi,

*Author to whom all correspondence should be addressed: E-mails: alavim@yahoo.com, alavi@aut.ac.ir; Phone: +982164543008; Fax: +982166414213

2019), sonochemical degradation (Abbasi and Razzaghi, 2008) and oxidation (Söğüt and Akgün, 2009). Among these methods, adsorption is the most promising and efficient due to its simplicity, low-cost, and ease of use on a large-scale combined with the possibility of adsorption regeneration/ recovery. (Al Nafiey et al., 2017; Ali et al., 2018; Ali et al., 2019a; Teymourian et al., 2021). Despite these features, the adsorption efficiency in this process is limited by the specific surface, non-selectivity, active sites, and adsorption kinetics (Ali et al., 2018; Sharma et al., 2015).

Presently, graphene oxide (GO) and its derivatives are considered the most suitable nano-adsorbents due to the high surface area and efficient adsorbent production (Ali et al., 2019c). However, the small size of nano-adsorbents, such as GO, can exacerbate the difficulty of their separation (regeneration/ recovery) from the environment (Sadegh et al., 2017). The addition of specific functional groups prevents the agglomeration of GO nano-adsorbents and has a significant influence on its properties, including capacity and adsorption rate, as well as analytical parameters, such as selectivity and tendency (Gu et al., 2018; Gul et al., 2016; Hu et al., 2016). Functionalized sulfonated graphene oxide (SGO) has recently been applied in the field of pharmaceutical chemistry and cell biology studies (Mondal, 2012). It has also been employed to attain increased efficiency in lithium-ion batteries (Li et al., 2012) and methanol fuel cells (Heo et al., 2013), improve electrochemical properties of the poly-ortho-aminophenol (Ehsani et al., 2017), and also dye removal from water (Scalese et al., 2016; Shen and Chen, 2015). However, to the best of our knowledge, SGO and its regeneration/ recovery in the adsorption process of BB41 has not been studied so far.

The main aim of this study is to assess the performance of functionalized graphene oxide nano-adsorbent added with 1,3 Propane Sultone and 1,4 Butane Sultone (GO/1,4-butane sultone (SGO_1) and GO/1,3-propane sultone (SGO_2)), which are heterocyclic compounds that can introduce alkyl chains with SO_3H- functionalities and can hence be utilized as sulfo alkylating agents (Mondal, 2012), for removal of BB41 dye from aqueous solution. The synthesis of the two nano-adsorbents and classical adsorption experiments were accomplished in order to investigate the effects of the main parameters, followed by related isotherm, kinetics, and thermodynamic studies. In addition, the regeneration/ recovery of the SGO_1 and SGO_2 were also assessed using a modified domestic microwave oven.

2. Materials and methods

2.1. Preparation and characterization of SGO_1 and SGO_2

Fig. 1 briefly demonstrates the procedure of preparing the two SGOs. The synthesis of GO from natural graphite was accomplished using the modified Hummer method (Kowsari and Mohammadi, 2016). To prepare the nano-adsorbents, dried graphene oxide (2 g) was added to 20 mL of dimethyl sulfoxide (DMSO) and 1-butyl 3-methylimidazolium bromide (4 g) and triphenylphosphine (1 g) were added to the solution and stirred. In the next step, hexamethylenediamine (2 g) was added to the resulting solution and thoroughly stirred at 140 °C for 12 hours using the stirrer. Eventually, the amine-functionalized graphene oxide (GOA) was chilled at room temperature and washed with 20 mL of dichloromethane (CH_2Cl_2). To synthesize SGO_1 and SGO_2, 1,4 butane sultone and 1,3 propane sultone (Sigma-Aldrich Corporation) were dissolved in DMSO, mixed with GOA and refluxed for 24 hours, separately. At last, two filtered SGO nano-adsorbents were washed with 20 mL of CH_2Cl_2 and dried in the oven. All the chemicals used as received without further purification from Merck & Co., Inc.

In order to characterize SGO_1 and SGO_2 nano-adsorbents, Scanning Electron Microscope (SEM), Brunauer-Emmett-Teller (BET), X-ray Crystallography (XRD), Raman spectroscopic, and Fourier-Transform Infrared Spectroscopy (FTIR) were performed. The XRD analysis was carried out using an X-ray diffractometer (Philips-Holland PW1730) with CuK_α radiation (λ = 1.5406 Å) at 40 kV, and FT-IR analysis was performed with a Nexus 670 (Thermo-USA) in the spectral range of 4000 to 8000 cm^{-1} using KBr discs. Raman spectroscopy was conducted using a Raman microscope (Renishaw-UK). The morphologies of SGO_1 and SGO_2 were observed by SEM (Seron Technology, AIS2100, South Korea) operating at 20 kV, and BET analysis was performed by N_2 adsorption/desorption isotherms at 77K using Belsorp mini II analyzer (Bel-Japan).

2.2. Adsorption experiments

BB41 was provided by Alvan Sabet Company (Iran), and its structure and assets are detailed in Table 1. The pH of the solution was adjusted with H_2SO_4 and NaOH and determined by a 340i/SET pH meter (WTW-Germany). All adsorption experiments were accomplished with 100 mL Erlenmeyer flasks using a batch technique, and the solution was agitated at 200 rpm with a standard shaker (Edward Buhler, Germany).

Afterward, the adsorption capacity was studied by dispersing a specific adsorbent dose using an ultrasonic bath (SonoSwiss, SW1H-Switzerland) for 3 minutes into 25mL of each specific initial dye concentration of BB41 aqueous solution, and the sample was centrifuged (Hettich, EBA 21-Germany) at 6000 rpm for 10 minutes for detachment of suspended particles (Karimifard and Alavi Moghaddam, 2016a).

It should be noted that in order to prevent the accumulation of nano-adsorbents, an ultrasonic bath was used before the dye solution and nano-adsorbent were placed on the orbital mixer. The use of the ultrasonic bath for over 10 minutes reduces the

removal efficiency due to the agglomeration of nanoparticles. Accordingly, a 3-minute sonication was considered in order to prevent excessive effects of sonication in dye removal and possible accumulation of nano-adsorbent. Additionally, a spectrophotometer (HACH, DR/400, USA) was utilized to measure the BB41 concentration at 609 nm (λ_{max}). The amount of dye adsorbed by the adsorbents (q) and the percentage of dye removal (R) were computed using Eqs. (1-2):

$$Dye\ removal\ efficiency\ (\%) = \frac{C_0 - C_f}{C_0} \times 100 \qquad (1)$$

$$Adsorption\ capacity\ (mg/g) = \frac{(C_0 - C_f)V}{M} \qquad (2)$$

where C_0 = the initial dye solution concentration (mg/L), C_f = the final solution concentration (mg/L), V = solution volume (L), and M = mass of adsorbents (g) (Baird, 2017).

It should be mentioned that since the concentration of BB41 solution decreases by 30% without adsorbent addition at high pH values (≥10), the dye removal mechanism does not only depend on the adsorption process.

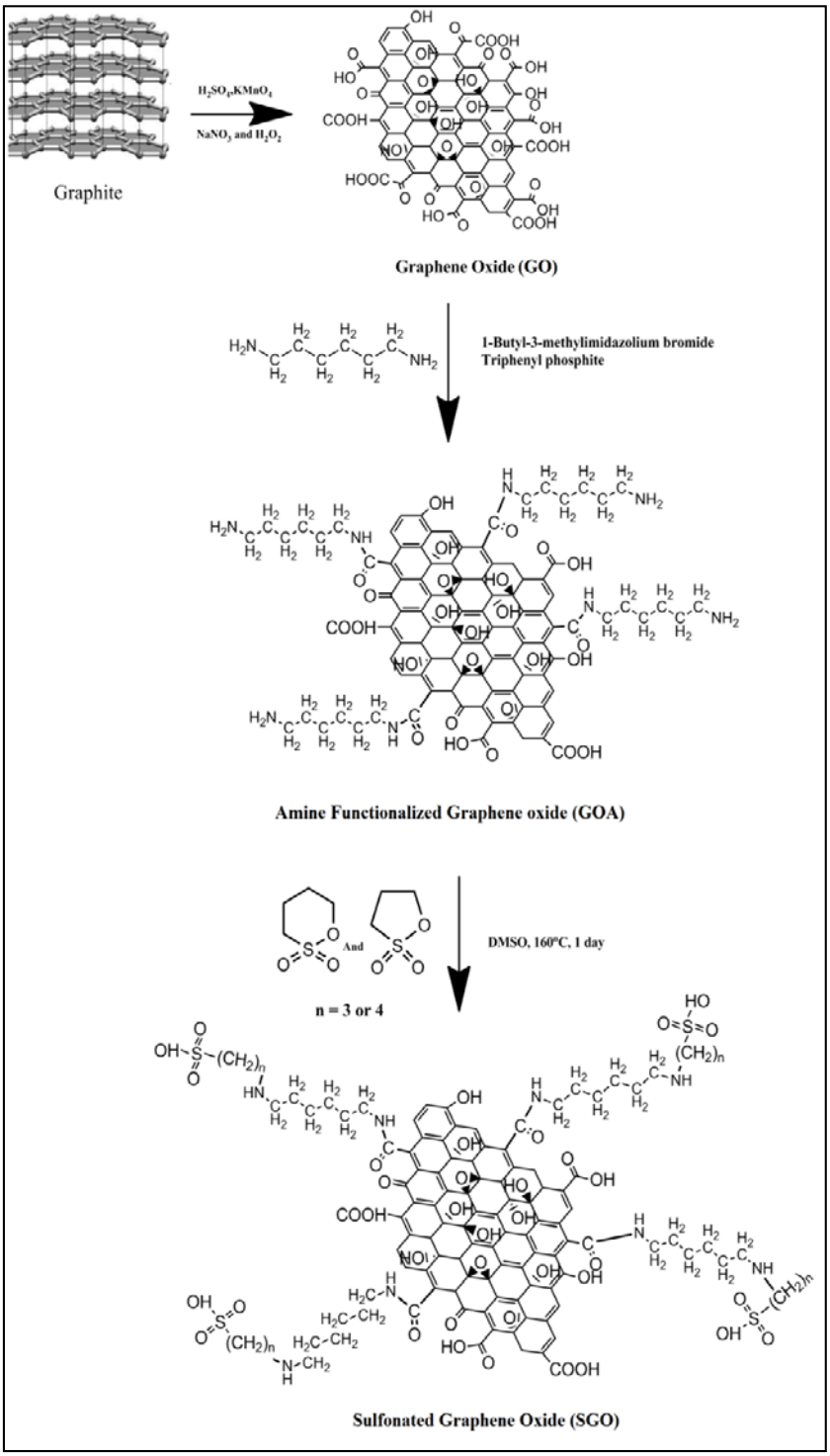

Fig. 1. Procedure of preparing sulfonated graphene oxides in the present study (SGO_1 and SGO_2)

Table 1. The structure and general properties of BB41

Characteristics	*Value*	*Chemical structure*
Molecular formula	$C_{20}H_{26}N_4O_6S_2$	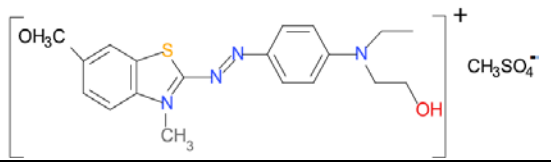
λ_{max} (nm)	609	
Molecular weight (MW)	482.57	

After adsorption experiments, process isotherm, kinetic, and thermodynamic were studied. Isotherm data were studied by fitting them into various equilibrium models (Ali et al., 2019c; Karimifard & Alavi Moghaddam, 2016a). To analyze the isotherm of BB41 adsorption onto SGO_1 and SGO_2, the Langmuir/ Freundlich/ Temkin/ Dubinin Radushkevich isotherm models were used.

Kinetic equations are utilized in order to predict and describe the behavior of the adsorbed molecules (per unit time) and/ or the adsorption rate (Tran et al., 2017). Herein, the kinetics of BB41 adsorption onto SGO_1 and SGO_2 were studied using two kinetic equations, Pseudo-First-Order/ Pseudo-Second-Order models.

The thermodynamic parameters indicate the spontaneity and feasibility, endothermic or exothermic reaction, and entropy changes during the adsorption process (Jaycock and Parfitt, 1981; Uğurlu, 2009). The thermodynamic parameters of adsorption, like standard enthalpy change ($\Delta H°$ (kJ/mol)), Gibbs free energy change ($\Delta G°$ (kJ/mol)), and standard entropy change ($\Delta S°$ (J/mol.K)), were also calculated (Lima et al., 2019).

Due to the economic cost and environmental problems associated with expensive adsorbents, the applicability of any adsorbents depends on their capability of regeneration/ recovery after the adsorption process should be considered (Ali et al., 2019b; Karimifard and Alavi Moghaddam, 2016b). Microwave regeneration has recently been considered as a novel thermal method due to its ability of molecular-level heating in addition to its energy and space saving capability, which leads to rapid and homogeneous regeneration of materials. This regeneration method was also studied previously in our research group (Karimifard and Alavi Moghaddam, 2016b; Shoushtarian et al., 2020).

In order to saturate the SGOs for regeneration/ reuse, the SGO_1 (0.015 g) and SGO_2 (0.02g) were added to the BB41 solution (50 and 100 mg/L) and stirred for 3 hours (Based on pre-tests), respectively. Then, to separate the saturated SGOs from the BB41 solution, the mixture was washed and filtered with double-distilled water and 0.2 µm filters (PTFE, Sartorius, Germany) and the saturated SGOs were dried at 80 ˚C for 8 hours in the oven. Thermal regeneration/ recovery of SGO_1 and SGO_2 (considering the carbonaceous base of the two nano-adsorbents) was then performed using modified domestic microwave oven according to Karimifard and Alavi Moghaddam (2016c) for four consecutive periods (Karimifard and Alavi Moghaddam, 2016b). The following equations were used to study regenerated SGOs adsorption capacities (Eqs. 3-4):

$$Regeneration\ Efficiency = RE(\%) = \frac{q_{reg}}{q_{initial}} \times 100 \quad (3)$$

$$Step\ Stripping\ Efficiency = SSE(\%) = \frac{q_{reg(i)}}{q_{initial(i-1)}} \times 100 \quad (4)$$

It should be noted that q_{reg} (mg/g) and $q_{initial}$ (mg/g) should be calculated after the regeneration process and at the initial conditions, respectively. (The regeneration cycle is represented by *i*).

3. Results and discussion

3.1. Characterization of SGO_1 and SGO_2

The SEM (Fig. 2) and BET tests were used to characterize the morphology and surface structure of the nano-adsorbents, respectively. As shown in the illustrations, the functional groups of the graphene oxide (1,3 propane sultone and 1,4 butane sultone) in this study have led to the formation of two-dimensional sheets with superficial surface roughness. The presence of sulfur (SO_3H-) in the structure of the two nano-adsorbents causes this roughness, which is considered to be useful for fortified interfacial interactions (Cao et al., 2018; Ch'Ng et al., 2016; Heo et al., 2013; Mohamadi et al., 2020).

In addition, according to the BET tests results, the specific surface area of SGO_1 (8.43 m^2/g) and SGO_2 (10.37 m^2/g) were reduced compared with that of pristine GO (38 m^2/g). The specific surface area decrease of functionalized GO could be due to its defective cutting as well as the massification of the particles during nano-adsorbents preparation (Abdi et al., 2017; Fang et al., 2014; Zhang et al., 2014).

Fig. 3 shows the structural properties of the two nano-adsorbents, including their XRD, FT-IR and Raman spectra. The typical diffraction peaks in the XRD pattern (Fig. 3a) were observed at 2θ= 24.45° and 43.13° for SGO_1 and 2θ= 24.57° and 42.91° for SGO_2, corresponding well to the (002) and (100) planes of reduced graphene oxide (rGO) according to the interpretations of similar studies (Loryuenyong et al., 2013; Seifvand and Kowsari, 2017).

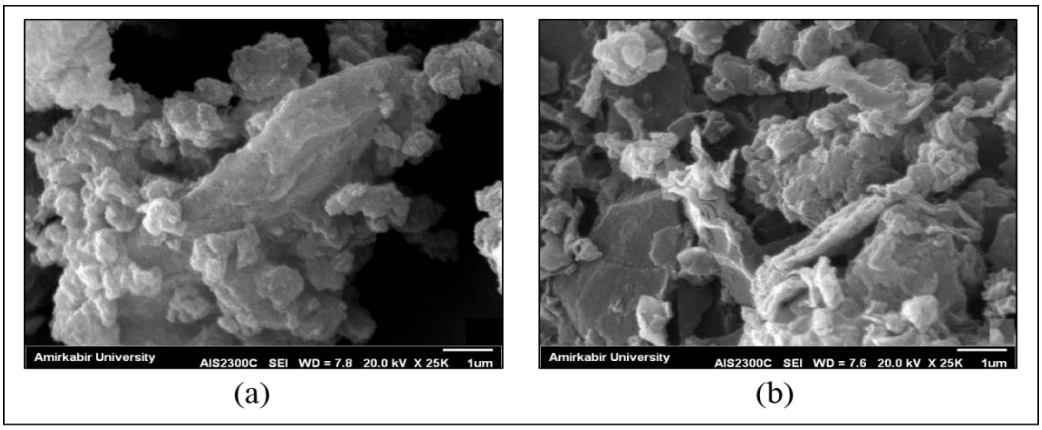

Fig. 2. SEM images of (a) SGO_1 and (b) SGO_2

The connections of the covalent functional groups are indicated by Raman spectra of SGO_1 and SGO_2 (Fig. 3b). The D band (mainly related to the sp^3 defects) and G band (related to the sp^2 bonded carbon atoms) are the essential bands of Raman spectroscopy for nano-adsorbents (Pant et al., 2016). The D and G bands intensity ratio (I_D/I_G), shows the defects found on the graphene surface (Seifvand and Kowsari, 2017). An increase in I_D/I_G ratio of SGO_1 (0.94) and SGO_2 (0.95) compared with GO (0.9) represents the crystalline growth. Also, according to Cao et al. (2018), the oxygenated functional groups decrease by establishing a covalent bond between the surface of the graphene oxide and the functional groups (Cao et al., 2018). Furthermore, based on the FT-IR spectrum results (Fig. 3c and Table 2), the functionalization of the graphene oxide with 1,3 propane sultone and 1,4 butane sultone was accomplished.

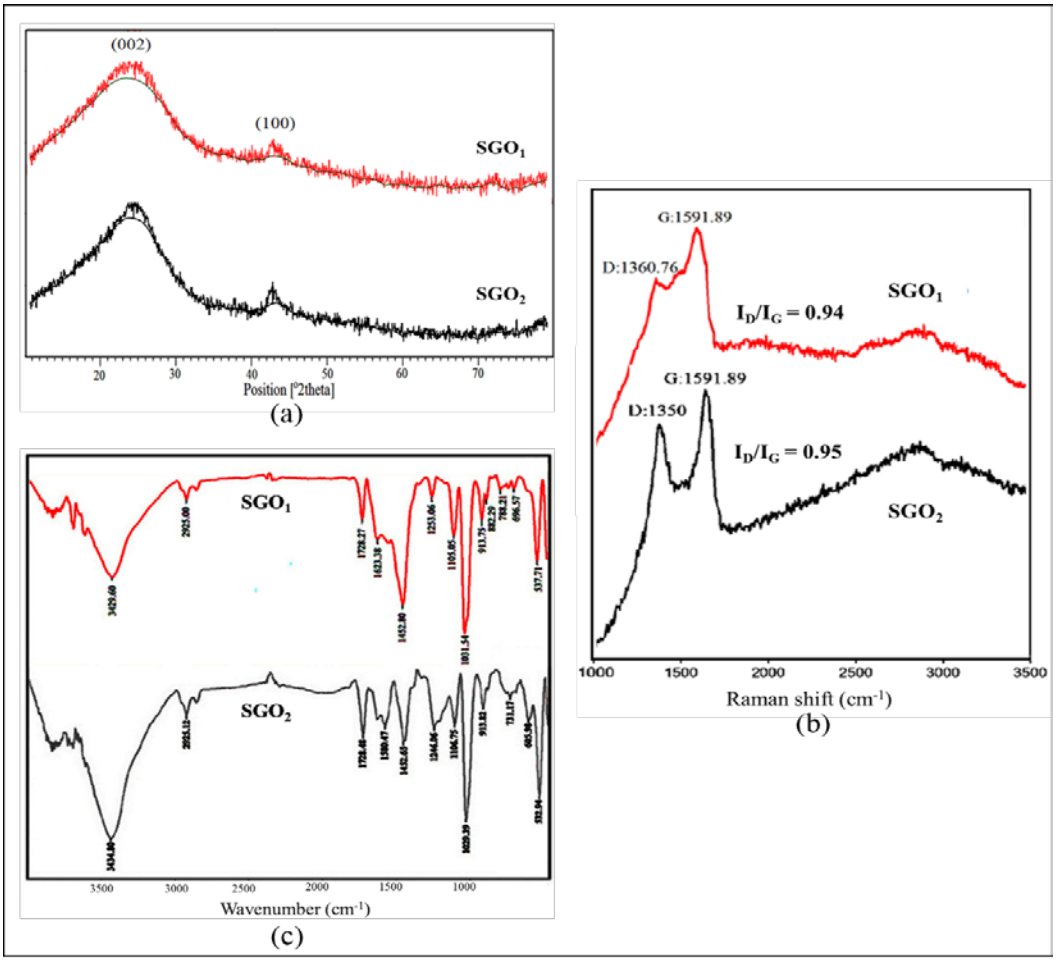

Fig. 3. Comparative structural properties of SGO_1 and SGO_2 (a) XRD patterns; (b) Raman spectrum; (c) FT-IR spectra

Table 2. FT-IR analysis based on the SGO_1 and SGO_2 bonds wavelengths, compared to the similar studies

Bonds type	***Wavelength (cm^{-1})***		***Similarly reported wavelength (cm^{-1}) Reference***
	SGO_1	***SGO_2***	
Hydroxyl stretching (OH)	3429	3434	3300-3500 Chen X. et al. (2017); Gu et al. (2018)
Aromatic (C-H)	2925	2925	2924 Zhang L. et al. (2018)
Carbonyl (C=O)	1728	1728	1728 Tajima et al. (2017)
Conjugated carbon (C=C)	1623	1580	1639 Chen L. et al. (2017)
Epoxy (C-O-C)	1452	1452	1445 Chen L.et al. (2017)
stretching vibration (C-OH)	1253	1246	1224 Tajima et al. (2017)
stretching vibration (C-N)	1105	1106	1132 Chen L. et al. (2017)
stretching vibration (S=O)	1031	1029	1029 and 1088 Beydaghi et al. (2014); Cao et al. (2018)
flexural vibration (C=C)	530-913	530-913	542-976 Tajima et al. (2017)

3.2. Effects of important parameters in BB41 adsorption onto SGO_1 and SGO_2

3.2.1. Effect of initial pH

As presented in Fig. 4a, the effect of initial pH on BB41 removal onto SGO_1 and SGO_2 was assessed in the range of 3 to 9 under the following conditions: Contact time= 60 and 30 minute, adsorbent dose= 0.2 and 0.15 g/L, and initial dye concentration= 50 and 100 mg/L, respectively. The BB41 removal efficiency and adsorption capacity (q) were increased from 43% (q= 142 mg/g) to 85% (q= 274 mg/g) for SGO_1 and 44% (q= 216 mg/g) to 90% (q= 434 mg/g) for SGO_2. This was partly resulted from the formation and augmentation of OH^- molecules with changing the pH values from 3 to 9 (get more negative). The increase in the adsorption process was also due to the competition between the BB41 dye molecules (with positive electric charges) and OH^- molecules (with negative charges) for adsorption sites on the surface of the SGOs (with negative charges).

In this competition, not only did the OH^- concentration decrease, but also the amount of BB41 adsorbed onto the SGOs increased. Due to the fact that increasing the pH values from 8 to 9 in both nano-adsorbents did not significantly change the dye removal efficiency, the optimum initial pH for both SGO_1 and SGO_2 was considered as 8 for the subsequent experiments.

3.2.2. Effect of initial BB41 concentration:

In the next stage of investigation of BB41 adsorption onto SGO_1 and SGO_2, the effect of the initial concentration of BB41 was evaluated under the following conditions: *Contact time* = 60 and 30 min, *adsorbent dose* = 0.2 and 0.15 g/L, and pH = 8, respectively. Under the mentioned conditions, in the process of BB41 removal using SGO_1, increasing the initial BB41 dye concentration led to a steady increase in the adsorption capacity (q) (presented in Fig. 4b) from 128 mg/g (C_0 = 20 ppm) to 333 mg/g (C_0 =125 ppm). Also, with SGO_2 the adsorption capacity increased from 123 mg/g (C_0 = 25 ppm) to 480 mg/g (C_0 = 200 ppm). Therefore, by applying the minimum removal of 80% and maximizing the adsorption capacity, the initial dye concentration of SGO_1 and SGO_2 was selected to be 50 and 100 ppm with an adsorption capacity of 279 and 421 mg/g, sequentially.

3.2.3. Effect of adsorbent dose

In this study, the adsorbent dose effect on BB41 adsorption, as one of the important parameters, was evaluated (Fig. 4c). The effects of SGO_1 and SGO_2 doses, ranging from 0.05 to 0.35 g/L, were investigated for the BB41 adsorption, as follows: Contact time= 60 and 30 minute, initial dye concentration= 50 and 100 mg/L, and pH= 8, respectively. The adsorption capacity decreased from 551 to 276 mg/g (using SGO_1) and 982 to 438 mg/g (using SGO_2) due to increase in SGO_1 and SGO_2 doses from 0.05 to 0.15 g/L and 0.05 to 0.2 g/L, respectively. Accordingly, SGO_1 and SGO_2 doses of 0.15 g/L and 0.2 g/L were considered (R> 80% and *q* maximum) for the subsequent experiments.

3.2.4. Effect of contact time

Figure 3d illustrates the effect of agitation time on the removal of BB41 using SGO_1 and SGO_2 with optimum values, resulting from previous stages, as follows: Adsorbent dose= 0.2 and 0.15 g/L, initial dye concentration= 50 and 100 mg/L, and pH= 8 respectively. Approximately 80% of dye adsorption on both nano-adsorbents occurred in the first 5 minutes (because of the ample active sites such as hydroxyl, carboxyl, and amino groups). The dye removal efficiency was relatively the same and above 80% with SGO_1 after 60 minutes and after 30 minutes with SGO_2; therefore, the optimum contact time of

BB41 adsorption with the nano-adsorbents were considered to be 60 and 30 minutes for SGO_1 and SGO_2 respectively.

3.2.5. Effect of temperature

Temperature increase leads to growth of the active site and flux of particles in the soluble phase (Liu et al., 2018). The BB41 dye removal capacity in the adsorption process (Fig. 4e) using SGO_1 and SGO_2 improved as the temperature was increased (10 °C to 70 °C), which indicates that the adsorption of BB41 using the two nano-adsorbents is thermo-sensitive. However, considering the before-mentioned constraints, the optimum temperature was selected to be 27°C (room temperature).

Subsequently, the maximum adsorption capacities of several studies evaluating BB41 adsorption were then compared in Table 3. Eventually, the maximum adsorption capacities of BB41 removal using SGO_1 and SGO_2 were 274 mg/g and 434 mg/g considering the optimum values mentioned above. The nano adsorbents used in this study were competitive and proper choices for BB41 removal compared with other adsorbents (Table 3).

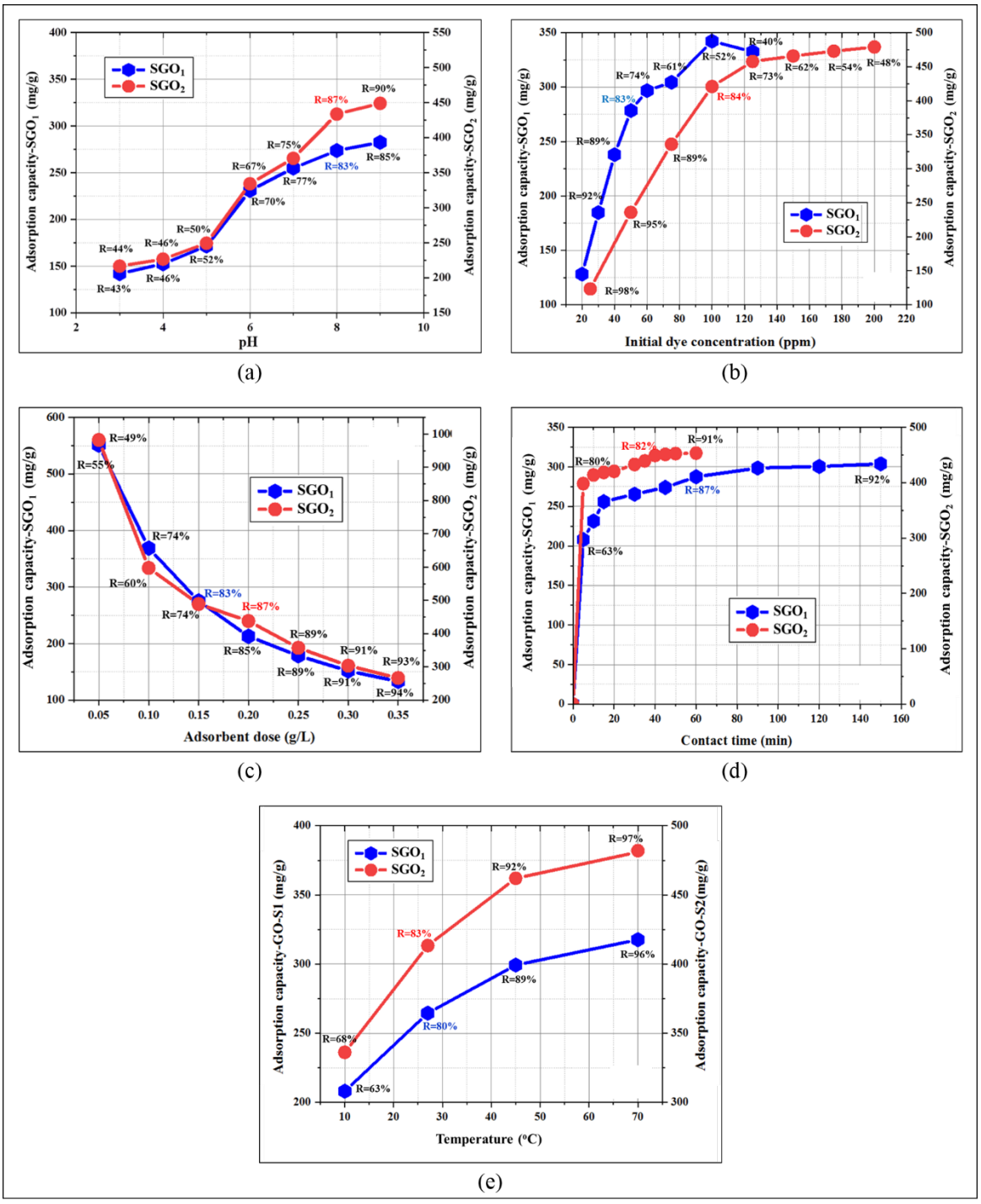

Fig. 4. The effect of Initial pH (a); Initial dye concentration (b); Adsorbents dose (c); Contact time (d); Temperature (e); on the adsorption process of BB41 using SGO_1 and SGO_2

Table 3. Comparison of the most considered adsorbents used to remove BB41

Adsorbent	*q (mg/g)*	*Reference*
Sodium Alginate	12	Yamini et al. (2018)
N, F-codoped flower-like TiO_2 Microspheres	143	Jiang et al. (2013)
Nanoporous Silica	345	Zarezadeh-Mehrizi and Badiei (2014)
Brick Waste	70	Kooli et al. (2015)
Reduced Graphene Oxide	143.6	Kimiagar et al. (2016)
Graphene Oxide/1,4 Butane Sultone (SGO_1)	274	Present study
Graphene Oxide/1,3 Propane Sultone (SGO_2)	434	Present study

3.3. Adsorption isotherms

The Langmuir, Freundlich, Temkin, and Dubinin-Radushkevich isotherm equations and main parameters for BB41 removal using SGO_1 and SGO_2 are reported in Table 4. The adsorption processes of the two nano-adsorbents follow the Langmuir isotherm with a correlation coefficient (R^2) of 0.9970 for SGO_1 and 0.9965 for SGO_2. Based on this compliance with the Langmuir isotherm, adsorption is more likely to occur in single layers and on specific active and homogeneity sites on the adsorbent surfaces.

It also shows that each active surface contains only one layer and has uniform adsorption energy (Ayawei et al., 2017).

3.4. Adsorption kinetics

The corresponding parameters of the pseudo-first-order and pseudo-second-order kinetics are presented in Table 5. BB41 adsorption using SGO_1 and SGO_2 coincides with the R^2 of 0.9995 (SGO_1) and 0.9994 (SGO_2) on the pseudo-second-order equation, which indicates that the BB41 adsorption onto both nano-adsorbents was a chemical process.

Table 4. The fitting parameters of adsorption isotherms for BB41 adsorption by SGO_1 and SGO_2

Isotherm model	*Equation*	*Equation factors definition*	*Fitting parameters*	*Nano-adsorbents*	
				SGO_1	*SGO_2*
Langmuir	$\frac{C_e}{q_e} = \frac{1}{K_L q_m} + \frac{C_e}{q_m}$	C_e = Dye concentration at equilibrium q_e = Adsorption capacity at equilibrium K_L = Langmuir constant q_m = maximum adsorption capacity	R^2	0.997	0.996
			q_{max} (mg/L)	333.34	454.54
			K_L (L/mg)	0.682	0.76
Freundlich	$ln\, q_e = ln\, K_F + \frac{1}{n} ln\, C_e$	K_F = Freundlich constant n = Adsorption intensity	R^2	0.898	0.936
			K_f (mg/g)-(L/mg)$^{1/n}$	157.32	181.39
			n	4.92	4.17
Temkin	$q_e = B_l\, ln\, K_T + B_l\, ln\, C_e$	B_l = Heat of adsorption dimensionless parameter K_T = Equilibrium binding constant	R^2	0.948	0.964
			K_T (L/mg)	29.35	18.61
			B_1 (m/g)	46.267	66.84
D-R	$ln\, q_e = ln\, q_s - 2BRT\, ln\, (1+ 1/C_e)$	B = Mean adsorption energy per unit of the adsorbed molecule ($E = (1/\sqrt{2B})$) T = Absolute temperature (Kelvin) R = Gas constant (8.31 J.mol^{-1}. k^{-1}) q_s = Saturation capacity	R^2	0.958	0.903
			q_s (mg/g)	321.43	436.71
			B (mol^2.j^2)	0.0003	0.0002
			E (kj/mol)	45.61	49.90

Table 5. The fitting parameters of the general-order kinetic model for BB41 adsorption using SGO_1 and SGO_2

Kinetic model	*Equation*	*Definition of factors in Equation*	*Fitting parameters*	*Nano-adsorbents*	
				SGO_1	*SGO_2*
Pseudo-first-order	$log(q_e - q_t) = log\, q_e - \frac{K_l}{2.303}t$	q_e = Adsorption capacity at equilibrium	R^2	0.949	0.955
		q_t = Adsorption capacity at time t (min).(mg/g)	k_1 (g/mg-min)	0.0341	0.0341
		k_1 = Pseudo-first-order rate constant	q_e (mg/g)	92.305	92.305
Pseudo-second-order	$\frac{t}{q_t} = \frac{1}{K_2 q_e^2} + \frac{1}{q_e}t$	k_2 = Pseudo-second-order rate constant	R^2	0.9995	0.9994
			k_2 (min^{-1})	0.0512	0.0046
			q_e (mg/g)	78.125	312.5

3.5. Adsorption thermodynamic

The linear regression diagrams of the thermodynamic equation are plotted based on Van't Hoff presented in Table 6. Positive values of ΔH and ΔS indicate that BB41removal using SGO_1 and SGO_2 is endothermic. Consequently, both nano-adsorbents could be effectively used in the dye adsorption process. Also, the decrease in ΔG with increasing temperature reveals that the adsorption process was spontaneous at higher temperatures and the negative values of ΔG point out that adsorption can be done at room temperature.

3.6. Regeneration/ Recovery of SGO_1 and SGO_2

In this study, SGO_1 and SGO_2 were regenerated/ reused (4 cycles) by microwave irradiation (Table 7). The adsorption capacity (q) decreased on a smooth basis following the subsequent regeneration cycles.

This downward trend could be attributed mainly to incomplete burning accumulation, which plays the role of undamaged waste material and changes the structures of the functional groups in the nano-adsorbents, leading to reduction in adsorption capacity.

4. Conclusions

In the present study, two functionalized sulfonated graphene oxide (GO/1,4-butane sultone (SGO_1) and GO/1,3-propane sultone (SGO_2)) were synthesized, and the success of the covalent functional groups' connections was confirmed by SEM, BET, XRD, FTIR, and Raman spectroscopy analysis.

Table 6. The thermodynamic parameters for BB41 adsorption by SGO_1 and SGO_2

Fitting parameters	*Equation*	*Equation factors definition*	*Nano-adsorbents*	
			SGO_1	*SGO_2*
ΔG (kJ/mol)	$\Delta G = -RTlnK_c$	R = Gas constant (8.31 $J.mol^{-1}.k^{-1}$) T = Absolute temperature (°K) K_c = Constant adsorption equilibrium	-1.1934 (T=283°)	-1.7 (T=283°)
			-3.3145 (T=296°)	-3.85 (T=296°)
			-5.7485 (T=318°)	-6.6 (T=318°)
			-8.5825 (T=343°)	-9.22 (T=343°)
ΔH (kJ/mol)	$\Delta H = \Delta G + T\Delta S$	-	32.9175	33.44
ΔS (J/K.mol)	$lnK_C = \frac{\Delta S}{R} - \frac{\Delta H}{RT}$	-	121.382	125.107
R^2	-	-	0.991	0.988
K_c (mg/L)	$K_C = (\frac{C_{Ae}}{100 - C_{Ae}})$	C_{Ae} = Amount adsorbed on solids at equilibrium	1.66 (T=283°)	2.05 (T=283°)
			3.845 (T=296°)	4.77 (T=296°)
			8.8 (T=318°)	12.15 (T=318°)
			20.27 (T=343°)	25.31 (T=343°)

Table 7. The different regeneration/ recovery periods of SGO_1 and SGO_2

Status	***SGO_1***			***SGO_2***		
	***q* (mg/g)**	**SSE (%)**	**RE (%)**	***q* (mg/g)**	**SSE (%)**	**RE (%)**
Raw	280	-	-	420	-	-
First period	195	69	69	386	91	91
Second period	174	89	62	350	90	83
Third period	150	86	53	315	90	75
Fourth period	124	82	44	295	93	61

The effects of the important parameters in BB41 adsorption onto SGO_1 and SGO_2 were evaluated with following conditions: pH=8, initial dyeBB41 concentration= 50 and 100 mg/L, adsorbent dose= 0.2 and 0.15 g/L and contact time= 60 and 30 minute at room temperature; resulting in *q*= 274 and 434 mg/L (with removal efficiency of 85% and 90% for SGO_1 and SGO_2), respectively. High adsorption capacity indicated that SGO_1 and SGO_2 were competitive and suitable nano-adsorbents for BB41 removal.

The Langmuir isotherm best described the BB41 adsorption onto the two nano-adsorbents (R^2=0.997 (SGO_1) and R^2= 0.996 (SGO_2)); the Pseudo-second Order kinetic model (R^2=0.9995 (SGO_1) and R^2=0.9994 (SGO_2)), and the thermodynamic study (R^2=0.991 (SGO_1) and R^2=0.988 (SGO_2)) did as well. At the last stages of the present study, the nano-adsorbents were regenerated/ recovered in 4 cycles and the regeneration efficiency decreased from 69% to 44% in SGO_1 (*q*=124 mg/L in fourth period), and from 91% to 61% in SGO_2 (*q*=295 mg/L in fourth period).

Eventually, the results showed that the SGO_2 nano-absorbent demonstrated higher adsorption capacity (434 mg/g) compared with SGO_1 (274 mg/g) and it was recovered more efficiently with the selected thermal regeneration method (modified domestic microwave oven). Moreover, the regenerated SGOs were still effective nano-adsorbents for BB41 removal, even after multiple regenerations/ reuses.

Acknowledgments

The authors appreciate Amirkabir University of Technology (Tehran Polytechnic) and West Azerbayjan water and wastewater for their financial support. In addition, the authors wish to thank Mr. Mahyar Ghanadi Shakerdabdollah (Former M.Sc student of AUT).

References

Abbasi M., Asl N.R., (2008), Sonochemical degradation of Basic Blue 41 dye assisted by nanoTiO_2 and H_2O_2, *Journal of Hazardous Materials*, **153**, 942–947.

Abdi J., Vossoughi M., Mahmoodi N.M., Alemzadeh I., (2017), Synthesis of amine-modified zeolitic imidazolate framework-8, ultrasound-assisted dye removal and modeling, *Ultrasonics Sonochemistry*, **39**, 550–564.

Al Nafiey A., Addad A., Sieber B., Chastanet G., Barras A., Szunerits, S., Boukherroub R., (2017), Reduced graphene oxide decorated with Co_3O_4 nanoparticles (rGO-Co_3O_4) nanocomposite: a reusable catalyst for highly efficient reduction of 4-nitrophenol, and Cr (VI) and dye removal from aqueous solutions, *Chemical Engineering Journal*, **322**, 375–384.

Ali I., Alharbi O.M.L., ALOthman Z.A., Al-Mohaimeed A.M., Alwarthan A., (2019a), Modeling of fenuron pesticide adsorption on CNTs for mechanistic insight and removal in water, *Environmental Research*, **170**, 389–397.

Ali I., Alharbi O.M.L., ALOthman Z.A., Alwarthan A., Al-Mohaimeed A.M., (2019b), Preparation of a carboxymethylcellulose-iron composite for uptake of atorvastatin in water, *International Journal of Biological Macromolecules*, **132**, 244–253.

Ali I., Mbianda X.Y., Burakov A., Galunin E., Burakova I., Mkrtchyan E., Grachev V., (2019c), Graphene based adsorbents for remediation of noxious pollutants from wastewater, *Environment International*, **127**, 160–180.

Ali I., Alharbi O.M.L., Tkachev A., Galunin E., Burakov A., Grachev V.A., (2018), Water treatment by new-generation graphene materials: hope for bright future, *Environmental Science and Pollution Research*, **25**, 7315–7329.

Baird R.B., (2017), *Standard Methods for the Examination of Water and Wastewater*, Rice E.W., Baird R.B., Eaton A.D., 23rd Edition, Vol. 1, American Public Health Association, Washington DC, USA.

Ayawei N., Ebelegi A.N., Wankasi D., (2017), Modelling and interpretation of adsorption isotherms, *Journal of Chemistry*, **2017**, 15-26.

Basheer A.A., (2018a), Chemical chiral pollution: impact on the society and science and need of the regulations in the 21st century, *Chirality*, **30**, 402–406.

Basheer A.A., (2018b), New generation nano-adsorbents for the removal of emerging contaminants in water, *Journal of Molecular Liquids*, **261**, 583–593.

Beydaghi H., Javanbakht M., Kowsari E., (2014), Synthesis and characterization of poly (vinyl alcohol)/sulfonated graphene oxide nanocomposite membranes for use in proton exchange membrane fuel cells (PEMFCs), *Industrial and Engineering Chemistry Research*, **53**, 16621–16632.

Boudechiche N., Fares M., Ouyahia S., Yazid H., Trari M., Sadaoui Z., (2019), Comparative study on removal of two basic dyes in aqueous medium by adsorption using activated carbon from Ziziphus lotus stones, *Microchemical Journal*, **146**, 1010–1018.

Cao N., Zhou C., Wang Y., Ju H., Tan D., Li J., (2018), Synthesis and characterization of sulfonated graphene oxide reinforced sulfonated poly (ether ether ketone)(SPEEK) composites for proton exchange membrane materials, *Materials*, **11**, 516.

Ch'Ng Y.Y., Loh K.S., Daud W.R.W., Mohamad A.B., (2016), Synthesis and characterization of sulfonated graphene oxide nanofiller for polymer electrolyte membrane, *IOP Conference Series: Materials Science and Engineering*, **160**, 12035.

Chen L., Li Y., Du Q., Wang Z., Xia,Y., Yedinak E., Ci L., (2017), High performance agar/graphene oxide composite aerogel for methylene blue removal, *Carbohydrate Polymers*, **155**, 345–353.

Chen X., Wang X., Wang S., Qi J., Xie K., Liu X., Li J., (2017), Furfuryl alcohol functionalized graphene for sorption of radionuclides, *Arabian Journal of Chemistry*, **10**, 837–844.

Ehsani A., Kowsari E., Ajdari F.B., Safari R., Shiri H.M., (2017), Sulfonated graphene oxide and its nanocomposites with electroactive conjugated polymer as effective pseudocapacitor electrode materials, *Journal of Colloid and Interface Science*, **497**, 258–265.

Fang F., Kong L., Huang J., Wu S., Zhang K., Wang X., Huang X.J., (2014), Removal of cobalt ions from aqueous solution by an amination graphene oxide nanocomposite, *Journal of Hazardous Materials*, **270**, 1–10.

Gu S.Y., Hsieh C.T., Yuan J.Y., Hsueh J.H., Gandomi Y.A., (2018), Amino-functionalization of graphene nanosheets by electrochemical exfoliation technique, *Diamond and Related Materials*, **87**, 99–106.

Gul K., Sohni S., Waqar M., Ahmad F., Norulaini N.A.N., AK M.O., (2016), Functionalization of magnetic chitosan with graphene oxide for removal of cationic and anionic dyes from aqueous solution, *Carbohydrate Polymers*, **152**, 520–531.

Heo Y., Im H., Kim J., (2013), The effect of sulfonated graphene oxide on sulfonated poly (ether ether ketone) membrane for direct methanol fuel cells, *Journal of Membrane Science*, **425**, 11–22.

Hu L., Yang Z., Cui L., Li Y., Ngo H.H., Wang Y., Du B., (2016), Fabrication of hyperbranched polyamine functionalized graphene for high-efficiency removal of Pb (II) and methylene blue, *Chemical Engineering Journal*, **287**, 545–556.

Weil K.G., (1981), *Chemistry of Interfaces*, Jaycock M.J., Parfitt G.D., (Eds.), 1st Edition, Ellis Horwood Limited Publishers, Chichester, England.

Jiang Y., Luo Y., Zhang F., Guo L., Ni L., (2013), Equilibrium and kinetic studies of CI Basic Blue 41 adsorption onto N, F-codoped flower-like TiO_2 microspheres, *Applied Surface Science*, **273**, 448–456.

Karimifard S., Alavi Moghaddam M.R., (2016a), Removal of an anionic reactive dye from aqueous solution using functionalized multi-walled carbon nanotubes: isotherm and kinetic studies, *Desalination and Water Treatment*, **57**, 16643–16652.

Karimifard S., Alavi Moghaddam M.R., (2016b), The effects of microwave regeneration on adsorptive performance of functionalized carbon nanotubes, *Water Science and Technology*, **73**, 2638–2643.

Karimifard S., Alavi Moghaddam M.R., (2016c), Enhancing the adsorption performance of carbon nanotubes with a multistep functionalization method: optimization of Reactive Blue 19 removal through response surface methodology, *Process Safety and Environmental Protection*, **99**, 20–29.

Khan T.A., Chaudhry S.A., Ali, I., (2015), Equilibrium uptake, isotherm and kinetic studies of Cd (II) adsorption onto iron oxide activated red mud from aqueous solution, *Journal of Molecular Liquids*, **202**, 165–175.

Kimiagar S., Rashidi N., Witkowski B.S., (2016), Basic Blue 41 removal by microwave hydrothermal reactor reduced graphene oxide, *Desalination and Water Treatment*, **57**, 27269–27278.

Kooli F., Yan L., Al-Faze R., Al-Sehimi A., (2015), Removal enhancement of basic blue 41 by brick waste from an aqueous solution, *Arabian Journal of Chemistry*, **8**, 333–342.

Kowsari E., Mohammadi M., (2016), Synthesis of reduced and functional graphene oxide with magnetic ionic liquid and its application as an electromagnetic-absorbing coating, *Composites Science and Technology*, **126**, 106–114.

Li B., Xu M., Li T., Li W., Hu S., (2012), Prop-1-ene-1, 3-sultone as SEI formation additive in propylene carbonate-based electrolyte for lithium ion batteries, *Electrochemistry Communications*, **17**, 92–95.

Lima E.C., Hosseini-Bandegharaei A., Moreno-Piraján J.C., Anastopoulos I., (2019), A critical review of the estimation of the thermodynamic parameters on adsorption equilibria. Wrong use of equilibrium constant in the Van't Hoof equation for calculation of thermodynamic parameters of adsorption, *Journal of Molecular Liquids*, **273**, 425–434.

Liu J., Wang Z., Li H., Hu C., Raymer P., Huang Q., (2018), Effect of solid state fermentation of peanut shell on its dye adsorption performance, *Bioresource Technology*, **249**, 307–314.

Loryuenyong V., Totepvimarn K., Eimburanapravat P., Boonchompoo W., Buasri A., (2013), Preparation and characterization of reduced graphene oxide sheets via water-based exfoliation and reduction methods, *Advances in Materials Science and Engineering*, **2013**, 273-277.

Mahmoodi N.M., Abdi J., (2019), Nanoporous metal-organic framework (MOF-199): Synthesis, characterization and photocatalytic degradation of Basic Blue 41, *Microchemical Journal*, **144**, 436–442.

Mahmoodi N.M., Hayati B., Arami M., (2012), Kinetic, equilibrium and thermodynamic studies of ternary system dye removal using a biopolymer, *Industrial Crops and Products*, **35**, 295–301.

Mohamadi M., Kowsari E., Yousefzadeh M., Chinnappan A., Ramakrishna S., (2020), Highly-efficient microwave absorptivity in reduced graphene oxide modified with PTA@ imidazolium based dicationic ionic liquid and fluorine atom, *Composites Science and Technology*, **188**, 107960.

Mohammadnia M., Naghizadeh A., (2016), Surveying of kinetics, thermodynamic, and isotherm processes of fluoride removal from aqueous solutions using graphene oxide nano particles, *Journal of Birjand University of Medical Sciences*, **23**, 29–43.

Mondal S., (2012), Recent developments in the synthesis and application of sultones, *Chemical Reviews*, **112**, 5339–5355.

Mubarak H.A., Kubba M.A., Hashim K., Al-Janabi A., Safaa K.H., (2021), A short review on dyes removal from water and wastewaters. *Materials Science and Engineering*, **1184**, 012017.

Pant B., Saud P.S., Park M., Park S.J., Kim H.Y., (2016), General one-pot strategy to prepare Ag–TiO_2 decorated reduced graphene oxide nanocomposites for chemical and biological disinfectant, *Journal of Alloys and Compounds*, **671**, 51–59.

Regti A., Laamari M.R., Stiriba S.E., El Haddad M., (2017), Removal of Basic Blue 41 dyes using Persea americana-activated carbon prepared by phosphoric acid action, *International Journal of Industrial Chemistry*, **8**, 187–195.

Roulia M., Vassiliadis A.A., (2005), Interactions between CI Basic Blue 41 and aluminosilicate sorbents, *Journal of Colloid and Interface Science*, **291**, 37–44.

Sadegh H., Ali G.A.M., Gupta V.K., Makhlouf A.S.H., Shahryari-ghoshekandi R., Nadagouda M.N., Megiel E., (2017), The role of nanomaterials as effective adsorbents and their applications in wastewater treatment, *Journal of Nanostructure in Chemistry*, **7**, 1–14.

Scalese S., Nicotera I., D'Angelo D., Filice S., Libertino S., Simari C., Privitera V., (2016), Cationic and anionic azo-dye removal from water by sulfonated graphene oxide nanosheets in Nafion membranes, *New Journal of Chemistry*, **40**, 3654–3663.

Seifvand N., Kowsari E., (2017), TiO_2/in-situ reduced GO/functionalized with an IL-Cr complex as a ternary photocatalyst composite for efficient carbon monoxide deterioration from air, *Applied Catalysis B: Environmental*, **206**, 184–193.

Sharma V.K., McDonald T.J., Kim H., Garg V.K., (2015), Magnetic graphene–carbon nanotube iron nanocomposites as adsorbents and antibacterial agents for water purification, *Advances in Colloid and Interface Science*, **225**, 229–240.

Shen Y., Chen B., (2015), Sulfonated graphene nanosheets as a superb adsorbent for various environmental pollutants in water, *Environmental Science and Technology*, **49**, 7364–7372.

Shoushtarian F., Moghaddam M.R., Kowsari E., (2020), Efficient regeneration/reuse of graphene oxide as a nanoadsorbent for removing basic Red 46 from aqueous solutions, *Journal of Molecular Liquids*, **312**, 113386.

Söğüt O.Ö., Akgün M., (2009), Removal of CI Basic Blue 41 from aqueous solution by supercritical water oxidation in continuous-flow reactor, *Journal of Industrial and Engineering Chemistry*, **15**, 803–808.

Sun X., Liu X., Yang B., Xu L., Yu S., (2015), Functionalized chrysotile nanotubes with mercapto groups and their Pb (II) and Cd (II) adsorption properties in aqueous solution, *Journal of Molecular Liquids*, **208**, 347–355.

Tajima K., Isaka T., Yamashina T., Ohta Y., Matsuo Y., Takai K., (2017), Functional group dependence of spin magnetism in graphene oxide, *Polyhedron*, **136**, 155–158.

Teymourian T., Alavi Moghaddam M.R, Kowsari, E., (2021), Performance of novel GO-Gly/HNTs and GO-GG/HNTs nanocomposites for removal of Pb (II) from water: optimization based on the RSM-CCD model, *Environmental Science and Pollution Research*, **4**, 1-18.

Tran H.N., You S.J., Hosseini-Bandegharaei A., Chao H.P., (2017), Mistakes and inconsistencies regarding adsorption of contaminants from aqueous solutions: a critical review, *Water Research*, **120**, 88–116.

Uğurlu M., (2009), Adsorption of a textile dye onto activated sepiolite. *Microporous and Mesoporous Materials*, **119**, 276–283.

Yamini Y., Faraji M., Rajabi A.A., Nourmohammadian F., (2018), Ultra efficient removal of basic blue 41 from textile industry's wastewaters by sodium dodecyl sulphate coated magnetite nanoparticles: removal, kinetic and isotherm study, *Analytical and Bioanalytical Chemistry Research*, **5**, 205–215.

Zarezadeh-Mehrizi M., Badiei A., (2014), Highly efficient removal of basic blue 41 with nanoporous silica, *Water Resources and Industry*, **5**, 49–57.

Zhang F., Wang B., He S., Man R., (2014), Preparation of graphene-oxide/polyamidoamine dendrimers and their adsorption properties toward some heavy metal ions, *Journal of Chemical and Engineering Data*, **59**, 1719–1726.

Zhang L., Li H., Lai X., Wu W., Zeng X., (2018), Hindered phenol functionalized graphene oxide for natural rubber, *Materials Letters*, **210**, 239–242.